AGU PUBLICATIONS

Geophysical Research Letters

RESEARCH LETTER

10.1002/2014GL060703

Key Points:
- First observation of modulation of PMSE at HF wavelengths by radio heating
- Qualitative and partial quantitative agreement with theoretical predictions

Correspondence to:
A. Senior,
a.senior@lancaster.ac.uk

Citation:
Senior, A., A. Mahmoudian, H. Pinedo, C. La Hoz, M. T. Rietveld, W. A. Scales, and M. J. Kosch (2014), First modulation of high-frequency polar mesospheric summer echoes by radio heating of the ionosphere, *Geophys. Res. Lett.*, *41*, doi:10.1002/2014GL060703.

Received 12 JUN 2014
Accepted 18 JUL 2014
Accepted article online 23 JUL 2014

First modulation of high-frequency polar mesospheric summer echoes by radio heating of the ionosphere

A. Senior[1], A. Mahmoudian[2], H. Pinedo[3], C. La Hoz[3], M. T. Rietveld[4], W. A. Scales[2], and M. J. Kosch[1,5]

[1]Department of Physics, University of Lancaster, Lancaster, UK, [2]Bradley Department of Electrical and Computer Engineering, Virginia Polytechnic Institute and State University, Blacksburg, Virginia, USA, [3]Department of Physics and Technology, University of Tromsø, Tromsø, Norway, [4]EISCAT Scientific Association, Ramfjordmoen, Norway, [5]South African National Space Agency, Hermanus, South Africa

Abstract The first high-frequency (HF, 8 MHz) observations of the modulation of polar mesospheric summer echoes (PMSE) by artificial radio heating of the ionosphere are presented and compared to observations at 224 MHz and model predictions. The experiments were performed at the European Incoherent Scatter facility in northern Norway. It is shown that model results are in qualitative and partial quantitative agreement with the observations, supporting the prediction that with certain ranges of ice particle radii and concentration, PMSE at HF radar wavelengths can be enhanced by heating due to the dominance of dust charging over plasma diffusion.

1. Introduction

Polar Mesospheric Summer Echoes (PMSE) are radar echoes from the vicinity of the Earth's mesopause observed at high latitudes during the summer. They are believed to originate from irregular structures in the electron density which are in turn caused by similar structures in the concentration of dust particles, mainly ice, which are charged by the attachment of plasma species. The observations and theory of PMSE have been reviewed by *Rapp and Lübken* [2004].

At the European Incoherent Scatter (EISCAT) facility in Norway, *Chilson et al.* [2000] discovered that the strength of PMSE could be modulated by heating the electrons with a powerful high-frequency radio wave. This effect was first explained by *Rapp and Lübken* [2000] and further studied by *Havnes et al.* [2003] and *Havnes* [2004] who predicted the response to heating on the basis of its effect on the dust charge and plasma diffusion and pointed out the utility of the technique for determining properties of the dust particles. Theoretical developments were made by *Scales* [2004], *Chen and Scales* [2005], *Biebricher et al.* [2012], and *Biebricher and Havnes* [2012] who extended the modeling of the response to longer wavelengths ($\geq$6 m) where the dust charging is expected to dominate plasma diffusion in controlling the behavior. Previous experiments have concentrated on modulation of PMSE at short wavelengths where diffusion is important and typically leads to a suppression of the PMSE during heating. At longer wavelengths, an enhancement is expected to be possible due to the increased dust charge.

To date, the EISCAT facility is the only one where the necessary combination of a high-power radio heating transmitter and radars of the appropriate wavelength exists to conduct these experiments and that has had results appear in the literature. Consequently, studies have been confined to the frequencies of the EISCAT VHF (224 MHz) and UHF (930 MHz) radars [*Rishbeth and van Eyken*, 1993], although unmodulated PMSE has been observed at frequencies as low as 2.78 MHz [*Bremer et al.*, 1996] using colocated instruments. Recently, the Mobile Rocket and Radar Observatory (MORRO) radar at 56 MHz [*La Hoz and Havnes*, 2008; *Pinedo et al.*, 2014] and an upgrade to the EISCAT HF facility to allow radar operations in addition to ionospheric heating has made routine work at longer wavelengths possible. In this study, the first observations at high frequencies (8 MHz) of the modulation of PMSE by radio heating are presented and compared with simultaneous observations at 224 MHz and predictions from the *Scales* [2004] model.

2. Experiment and Data

On 26 July 2013, the EISCAT HF Facility [*Rietveld et al.*, 1993] at Ramfjordmoen, Norway (69.6°N, 19.2°E), heated the ionosphere by radiating vertically in *O*-mode polarization at 6.77 MHz with an effective radiated

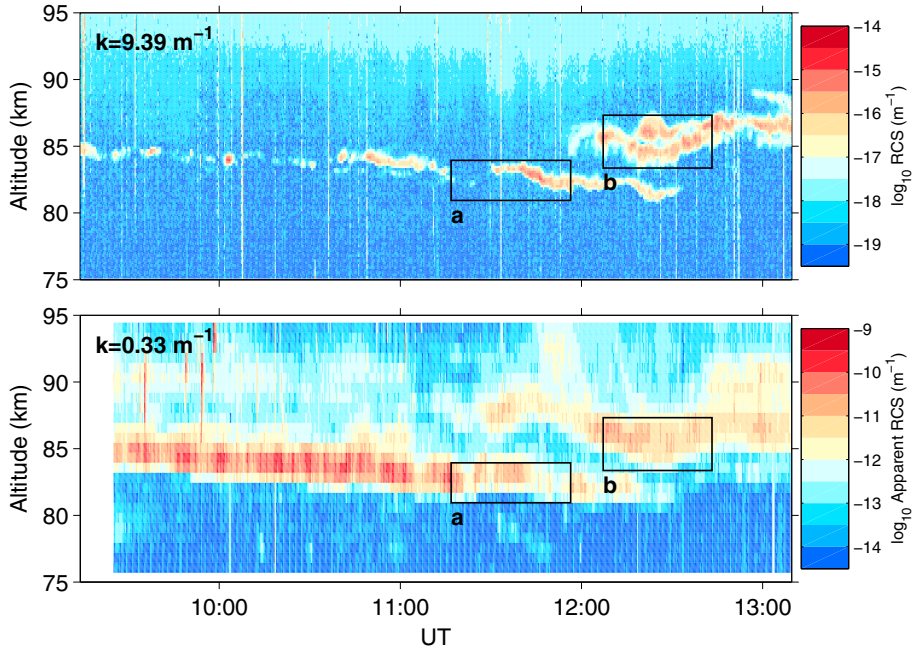

Figure 1. Observed radar cross sections from the (top) VHF and (bottom) HF radars on 26 July 2013. The black rectangles labeled "a" and "b" indicate the regions analyzed in more detail. The backscattering irregularity wave number *k* is marked in each frame.

power (ERP) of 601 MW using 10 transmitters on Array 1. All ERP estimates here assume a perfectly reflecting ground. This transmission was cycled 48 s on and 168 s off starting at 09:00 UT.

Simultaneously, the Facility operated in radar mode radiating vertically using two transmitters at 7.953 MHz on Array 1. The radar transmission used a pair of 20 baud complementary codes with 10 μs bauds (1.5 km range resolution) and alternated between *O*- and *X*-mode polarization with an ERP of 38 MW. A complete measurement cycle took 80 ms. Echoes were received using Array 3 in two orthogonal linear polarizations which were received digitally and combined in software to produce *O* or *X* polarization. The receiving antenna *O*-mode gain was 25.2 dBi. In this study, only *O*-mode-transmitted pulses received using *O*-mode polarization are used.

Additionally, the EISCAT VHF and UHF radars [*Rishbeth and van Eyken*, 1993], colocated with the HF Facility, operated vertically measuring the ionosphere at 224 MHz and 930 MHz, respectively, with a range resolution of 360 m using version 4 of the *manda* scheme. Due to the use of alternating codes [*Lehtinen and Häggström*, 1987], a complete measurement cycle took 192 ms. In this study, the UHF measurements were used only for determining the background electron density.

Figure 1 shows the observed radar cross sections per unit volume (RCS) from the VHF and HF radars during the whole of the experiment. The RCS at 7.953 MHz is typically 5–6 orders of magnitude greater than that at 224 MHz. Note that the HF RCS is referred to as "apparent RCS" because it has not been corrected for the effect of ionospheric absorption of the HF radar beam. The true RCS is higher than the apparent RCS by about a factor of 2 in this case. The VHF radar is not significantly affected by absorption. PMSE can be seen between 80 and 90 km throughout the interval with similar morphology at HF and VHF. The enhanced VHF RCS toward the upper altitude limit shown is due to incoherent scatter from ionospheric electrons [*Evans*, 1969]. The "tails" of enhanced RCS above the strong PMSE layers at HF are due to off-zenithal scattering from the PMSE layer.

During the subinterval "a" 11:16:48–11:56:24 UT and altitude range 80.9–83.9 km marked by a rectangle in Figure 1, the apparent HF RCS was found to be enhanced during radio heating and recovered to its preenhancement level after heating was stopped. Both before and after this subinterval, the HF RCS showed less clear evidence of modulation which was mostly suppression during heating. Subinterval "b," 12:07:12–12:43:12 and altitude range 83.4–87.3 km, also marked in Figure 1, is an example of this.

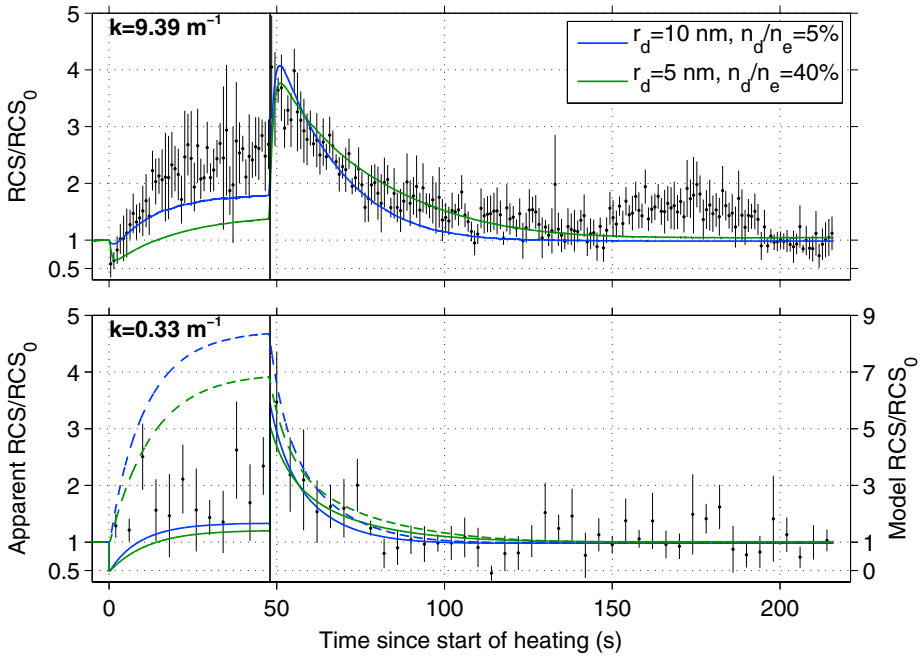

Figure 2. Median change in RCS over a heating cycle during subinterval a for the (top) VHF and (bottom) HF radars. The vertical line at 48 s after start of heating indicates when heating ceased. The time resolution is 0.96 s for the VHF and 4 s for the HF radar. The backscattering irregularity wave number k is marked in each frame. The error bars show the standard error of the median RCS. In both frames, the solid blue and green lines correspond to modeled RCS variations for dust parameters of $r_d = 10$ nm, $n_d/n_e = 5\%$ and $r_d = 5$ nm, $n_d/n_e = 40\%$, respectively. In Figure 2 (bottom), the dashed blue and green lines show the modeled RCS variations without corrections for observational effects; refer to the right-hand scale for these lines.

These subintervals were analyzed by performing a superposed-epoch analysis of the RCS from both radars over the heating cycles in them. First, the RCS was integrated over the altitude range and the logarithm taken. An undisturbed baseline was estimated by filtering the log-RCS time series with a boxcar filter equal in length to the heating cycle (216 s), thereby removing the heater-induced modulation. The baseline was then subtracted from the log-RCS to reveal the modulation and the median over all cycles in a subinterval were found (10 cycles in subinterval a, 9 in b). Subtracting the baseline also removes the mean of each cycle and results in the baseline-subtracted log-RCS not returning to zero at the end of a heating cycle when the disturbance has relaxed, since the mean of the modulation is generally nonzero. This was corrected by finding the mean of the last 24 s of the heater-off period in the epoch median and subtracting this from the epoch median. Data points with relative errors in the RCS exceeding 0.1 were excluded from the median in order to eliminate data where the PMSE was weak and the modulation ill defined. In subinterval a, 18% of the VHF data were excluded on this basis, mainly due to the weak PMSE at the start of the subinterval. In subinterval b only one point was excluded (0.05%). No HF data were excluded. Figures 2 and 3 show the results of this analysis in terms of the ratio RCS/RCS$_0$, where RCS$_0$ is the baseline, undisturbed RCS. The VHF RCS is plotted with a time resolution of 0.96 s and the HF RCS with a time resolution of 4 s.

In subinterval a, at VHF, the RCS is sharply suppressed at heater-on but recovers strongly during heating quickly exceeding the preheating level. At heater-off, there is a further enhancement ("turn-off overshoot") and then a gradual recovery to the preheating level. This behavior is qualitatively consistent with the model of *Havnes et al.* [2003] who also showed the first observations, although the strong recovery during heating is unusual. Between 150 and 200 s after the start of the heating cycle, an increase in the RCS is observed. This feature is thought to be an artifact of natural variations in the backscatter power which have not been completely removed in the analysis.

At HF, the RCS is enhanced at heater-on and remains so until heater-off when there is some evidence of a further enhancement and then a clearer decay back to the preheating level. This behavior is qualitatively consistent with that predicted by *Chen and Scales* [2005], *Mahmoudian et al.* [2011], and *Biebricher and Havnes* [2012]. Note that the reduction in the HF radar transmitter power due to power supply loading when

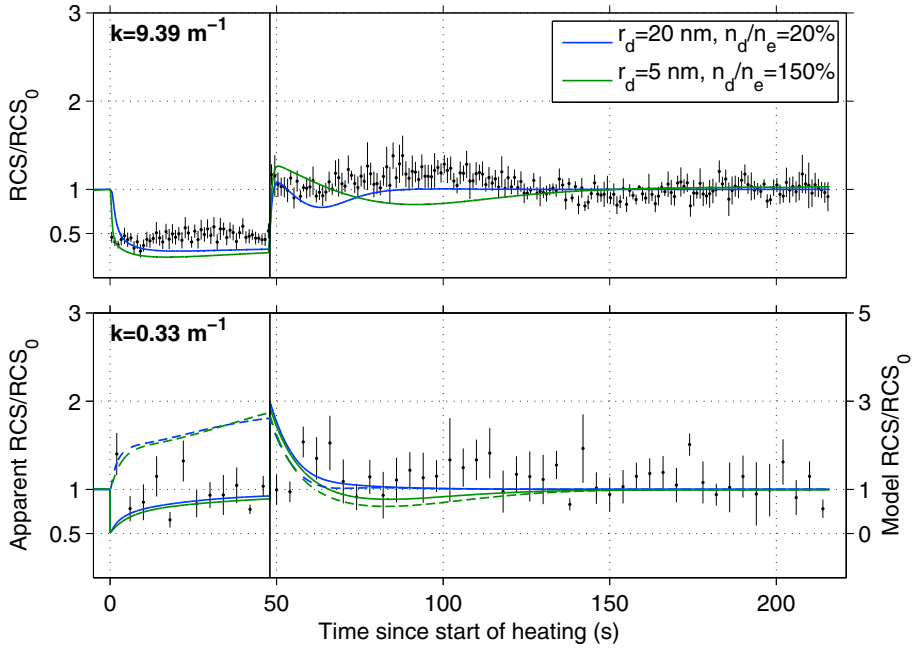

Figure 3. As Figure 2 but for subinterval b. In both frames, the solid blue and green lines correspond to modeled RCS variations for dust parameters of $r_d = 20$ nm, $n_d/n_e = 20\%$ and $r_d = 5$ nm, $n_d/n_e = 150\%$, respectively. In Figure 3 (bottom), the dashed blue and green lines show the modeled RCS variations without corrections for observational effects; refer to the right-hand scale for these lines.

the HF heating transmitters are in operation has not been allowed for. This reduction is thought to be less than 10%.

In subinterval b, at VHF, RCS again shows a sharp suppression at heater-on and remains suppressed until heater-off where it returns to the preheating level with a possible small turn-off overshoot. Gradual wavelike variations in the RCS throughout the cycle are again thought to be due to natural variations in the PMSE. At HF, there is a modest indication of suppression of the backscatter power during heating, but otherwise there are no clear heater-induced modulation effects.

3. Modeling

The model originally described by *Scales* [2004] and subsequently used and developed by *Chen and Scales* [2005], *Scales and Chen* [2008], and *Mahmoudian et al.* [2011] was used to interpret the observations in terms of mesospheric dust particle parameters. Hereinafter it is referred to as the "S04" model. In the modeling, the electron to ion temperature ratio during heating, T_e/T_i was assumed to be 2.5 in the center of the heated volume, which is probed by the VHF radar. The choice of this value of T_e/T_i is discussed later in this section. For subinterval a, the ambient electron density N_e was taken as 4×10^9 m^{-3} and for subinterval b a density of 3×10^9 m^{-3} in accordance with the VHF and UHF radar observations. The model was run for a range of dust radii r_d and ratios of dust density to electron density n_d/n_e. For subinterval a, the closest matches to the VHF observations were found by inspection of the array of results to be $r_d = 10$ nm and $n_d/n_e = 5\%$ and $r_d = 5$ nm and $n_d/n_e = 40\%$. For subinterval b, the closest matches were $r_d = 20$ nm and $n_d/n_e = 20\%$ and $r_d = 5$ nm and $n_d/n_e = 150\%$. These dust radii and densities are compatible with those found during in situ rocket measurements [*Rapp et al.*, 2009; *Robertson et al.*, 2009], lidar observations [*Baumgarten et al.*, 2008; *Baumgarten and Fiedler*, 2008], and radar observations of unmodulated PMSE [*Li et al.*, 2010], although these measurements do not fully resolve the concentration of particles as a function of radius. The square of the ratio of the electron density perturbation amplitude to its preheating level, $(\delta_{ne}/\delta_{ne0})^2$, which is proportional to the RCS, is plotted in Figures 2 and 3 (top) as the blue and green lines for the respective dust radii and density combinations.

The dashed blue and green lines in Figures 2 and 3 (bottom) (refer to right-hand scale) show the modeled HF RCS variation for $T_e/T_i = 2.5$ and the same dust parameters used for the VHF case. It is very obvious that

the model greatly overestimates the observed response, and this is due to two factors. First, the HF radar has a relatively wide beam (4° east-west, 9° north-south for the two-way pattern) compared to the size of the heated volume (heater beam width 6°E-W, 7°N-S) which means that the variation of T_e/T_i throughout the measured region must be accounted for since the radar averages over regions of plasma which have been heated to different degrees and which will therefore produce different RCS responses to heating. Second, the absorption of the HF radar beam in the *D* region is significant and is modulated by the change in T_e due to heating.

The model of *Senior et al.* [2010] was used to find the distribution of T_e throughout the heated volume as well as the horizontal variation of T_e/T_i through the PMSE layer. The modeled T_e permitted the changes in HF radar absorption to be estimated. The modeled T_e/T_i was used to run the S04 model for a range of T_e/T_i to simulate the variation in modulation of the PMSE across the heater beam. The theoretical HF radar observations were then determined by calculating the total backscatter power received by the radar considering the contributions from the modulated PMSE with different T_e/T_i, the absorption and the gain pattern of the radar. The result is plotted as the solid blue and green lines in Figures 2 and 3 (bottom) (refer to left-hand scale). It is clear that the modeled RCS variation is now in much closer agreement with the observations.

In subinterval a, the *D* region heating model predicted $T_e/T_i = 2$ at 82.5 km, the center of the PMSE altitude range used. Using this value in the S04 model produces RCS perturbations which are too small in amplitude to fit the observations. At 81 km, the bottom of the altitude range, the model gives $T_e/T_i = 2.5$, and this value was found to give a much better match to the observations. The heating model results for 81 km were therefore used in the analysis described above. In subinterval b, the model predicted $T_e/T_i = 2.5$ at 85 km, the center of the PMSE range for this subinterval. In this case, the amplitude of the modeled RCS variations were close to the observations, and so $T_e/T_i = 2.5$ was again used in the analysis. A justification of these choices is given in the next section.

4. Discussion

4.1. Subinterval a

As stated in section 3, the dust parameters used in the S04 model were chosen to fit the VHF observations. It is noteworthy that the S04 model results for HF with the same parameters fit the HF observations with a similar degree of success. At VHF, the green line ($r_d = 5$ nm and $n_d/n_e = 40\%$) provides the better fit after heating is turned off, but at HF it is difficult to distinguish between the two cases. For both VHF and HF the fits are least good during the period of heating. As noted in section 2, the strong recovery exceeding the preheating level during heating at VHF is unusual, but consistent with strong dust charging. Both model cases underestimate the increase in RCS, but the blue line ($r_d = 10$ nm and $n_d/n_e = 5\%$) is the closest match and corresponds to a case where the charging time scale is small compared to the diffusion time scale, leading to charging behavior dominating [*Chen and Scales*, 2005]. In the VHF case the model predicts a small initial decrease in RCS due to the increased diffusion, but the observed decrease is greater. In the HF case, the model also predicts a strong initial decrease due to the increased absorption of the HF radar beam (but recall from section 3 that the S04 model itself predicts a strong increase during heating due to dust charging). This is not observed, which may be partly due to the 4 s integration time. Disagreement between model and observations during heating could be an indication that the representation of the dust particle charging physics in the model needs to be refined.

Two other parameters which influence the S04 model results are the plasma recombination coefficient and the ion-neutral collision frequency, which were taken as 10^{-12} m^3 s^{-1} and 10^5 s^{-1}, respectively. These values are similar to those previously determined from observations [*Gledhill*, 1986; *Turunen et al.*, 1988]. *Mahmoudian et al.* [2011] found that varying the collision frequency can have a significant effect on the model results due to its influence on plasma diffusion. Ideally, these parameters should be based on measurements pertaining to the time of the experiment, and it is hoped that in a future study the incoherent scatter radar data can be used to constrain them.

Although the *Biebricher and Havnes* [2012] model was not used in this study, its predictions for long wavelengths such as 8 MHz appear qualitatively consistent with those of the S04 model and so are likely to be at least qualitatively consistent with the observations presented here.

4.2. Subinterval b

In this subinterval, the VHF RCS remained strongly suppressed throughout the period of heating. In contrast to subinterval a, this suggests a lack of significant additional dust charging during heating, which is also consistent with the small turn-off overshoot. The S04 model results match this behavior reasonably closely, except for a more gradual suppression at heater-on. It is not clear if the predicted damped oscillation in the RCS after heater-off is observed in the data or not. At HF, the S04 model correctly predicts a modest suppression of the RCS during heating, though the predicted sharp suppression at heater-on is again not observed. The model predicts that a turn-off overshoot should be observed as the heater-induced absorption increase is lost and the dust discharges, but this is not clearly observed. Overall, the model-observation agreement at HF is worse than in subinterval a, but the qualitative expectation that the modulation at HF should be weak in the absence of significant additional dust charging is consistent with the observations.

During subinterval b, the UHF radar observed a "biteout" in the electron density profile in the altitude range of the PMSE [*Li and Rapp*, 2013]. The electron density in the minimum of the biteout was 2×10^9 m^{-3} compared to the 3×10^9 m^{-3} at the surrounding altitudes. If the missing negative charge is due to the electrons attached to the dust, the total dust charge density is then 1×10^9 m^{-3}. In the S04 model, a 20 nm radius dust particle is taken to have an equilibrium charge number of −2 and for 5 nm radius, −0.5. This implies a dust particle density of 5×10^8 m^{-3} for 20 nm particles, which is 17% of the electron density in the region surrounding the PMSE layer. This agrees well with the value of $n_d/n_e = 20\%$ used in the model. For 5 nm particles, the density becomes 2×10^9 m^{-3}, or 67% of the ambient electron density, which is not in good agreement with the observed biteout. In subinterval a, no clear biteout was seen, but some PMSE was observed by the UHF radar making detection of a biteout difficult [*Li and Rapp*, 2013].

4.3. Sources of Error

The superposed-epoch analysis, like any use of averaging to reduce variance in data, assumes that the process being observed remains statistically stationary during the interval of averaging. The fact that PMSE modulation was very different in the subintervals studied shows that dust parameters did vary with time. In the event of such variation, it is unreasonable to expect a model to reproduce the observations exactly.

As T_e/T_i is difficult to measure, it is estimated by modeling the heating of the *D* region by the high-power radio wave. Besides any deficiencies in the model physics, the accuracy of the result is dependent on an accurate input electron density profile. For both the VHF and UHF radars, a profile was found by integrating the measurements over each 168 s heater-off period during the interval studied and taking the median. The final profile used was the mean of these VHF and UHF radar profiles, weighted according to the reciprocal of their variances. The absolute accuracy of the densities was calibrated at the *E* region peak against the f_oE obtained from the EISCAT Dynasonde and colocated Tromsø Digisonde ionosondes. It is estimated that a systematic error in the densities of ±5% may remain. For subinterval a, reducing the densities by 5% causes T_e/T_i to increase to 2.1 at 82.5 km and to 2.9 at 81 km, whereas increasing them by 5% gives 1.8 at 82.5 km and 2.3 at 81 km. The standard deviation of T_e/T_i due to the random error in the electron densities is estimated to be ±0.1. For subinterval b the ±5% calibration uncertainty leads to a range of 2.2–2.9 in T_e/T_i at 85 km, and the standard deviation due to random error is 0.2.

Additionally, the UHF radar measurements are susceptible to a systematic error below 80 km because the low electron densities (on the order of 10^9 m^{-3} or less) and wide receiver bandwidth mean that the incoherent scatter electron line contributes a significant fraction of the received power. This is not fully accounted for in the analysis software, leading to an overestimation of the electron density by up to 25%. Since the densities used are a weighted mean of those from the VHF and UHF radars and the weights are similar, the electron density may be overestimated by up to 12.5%. For subinterval a, reducing the densities in the 70–80 km interval, where the heater wave loses most of its power flux, by this amount results in T_e/T_i increasing to 2.2 at 82.5 km and 3.2 at 81 km. For subinterval b, T_e/T_i at 85 km increases to 3.2. Considering these anticipated errors in the modeled T_e/T_i, the use of a value of 2.5 in the S04 model in order to obtain better quantitative agreement with the observations in subinterval a seems reasonable.

The modeling of the HF observations also requires models of the heater and radar antenna gain patterns. Deficiencies in these could adversely affect the comparison between the HF observations and the S04 model results.

5. Conclusions

The first observations of the modulation of high-frequency PMSE by radio heating of the ionosphere have been presented. The interpretation of the present HF radar observations is complicated by the wide beam width which necessitates modeling of the spatial distribution of the ionospheric heating due to the finite size of the heater beam. Nevertheless, it has been shown that the observed behavior is in qualitative and partial quantitative agreement with the model of *Scales* [2004] and is likely to be in at least qualitative agreement with that of *Biebricher and Havnes* [2012]. This supports the results of current models which predict enhancement of PMSE during heating at long wavelengths due to the dominance of dust charging over diffusion for certain ranges of ice particle radii and concentration, as shown, for example, by *Mahmoudian et al.* [2011].

Acknowledgments

This work was supported by the Natural Environment Research Council (grant NE/I027231/1). EISCAT is an international association supported by China, Finland, Japan, Norway, Sweden, and the UK. Data are available through the EISCAT website (https://www.eiscat.se/groups/datahandling). The Tromsø digisonde is jointly owned and operated by QinetiQ and Tromsø Geophysical Observatory, and the ionograms were obtained through the University of Massachusetts Lowell GIRO database (http://spase.info/VWO/DisplayData/GIRO/GRM.PT15M).

The Editor thanks two anonymous reviewers for their assistance in evaluating this paper.

References

Baumgarten, G., and J. Fiedler (2008), Vertical structure of particle properties and water content in noctilucent clouds, *Geophys. Res. Lett.*, *35*, L10811, doi:10.1029/2007GL033084.

Baumgarten, G., J. Fiedler, F.-J. Lübken, and G. von Cossart (2008), Particle properties and water content of noctilucent clouds and their interannual variation, *J. Geophys. Res.*, *113*, D06203, doi:10.1029/2007JD008884.

Biebricher, A., and O. Havnes (2012), Non-equilibrium modeling of the PMSE Overshoot Effect revisited: A comprehensive study, *J. Plasma Phys.*, *78*, 303–319, doi:10.1017/S0022377812000141.

Biebricher, A., O. Havnes, and R. Bast (2012), On the necessary complexity of modeling of the polar mesosphere summer echo overshoot effect, *J. Plasma Phys.*, *78*, 225–239, doi:10.1017/S0022377811000596.

Bremer, J., P. Hoffmann, A. H. Manson, C. E. Meek, R. Rüster, and W. Singer (1996), PMSE observations at three different frequencies in northern Europe during summer 1994, *Ann. Geophys.*, *14*, 1317–1327.

Chen, C., and W. A. Scales (2005), Electron temperature enhancement effects on plasma irregularities associated with charged dust in the Earth's mesosphere, *J. Geophys. Res.*, *110*, A12313, doi:10.1029/2005JA011341.

Chilson, P. B., E. Belova, M. T. Rietveld, S. Kirkwood, and U.-P. Hoppe (2000), First artificially induced modulation of PMSE using the EISCAT heating facility, *Geophys. Res. Lett.*, *27*, 3801–3804.

Evans, J. V. (1969), Theory and practice of ionosphere study by Thomson scatter radar, *Proc. IEEE*, *57*(4), 496–530.

Gledhill, J. A. (1986), The effective recombination coefficient of electrons in the ionosphere between 50 and 150 km, *Radio Sci.*, *21*(3), 399–408.

Havnes, O. (2004), Polar mesospheric summer echoes (PMSE) overshoot effect due to cycling of artificial electron heating, *J. Geophys. Res.*, *109*, A02309, doi:10.1029/2003JA010159.

Havnes, O., C. La Hoz, L. I. Næsheim, and M. T. Rietveld (2003), First observations of the PMSE overshoot effect and its use for investigating the conditions in the summer mesosphere, *Geophys. Res. Lett.*, *30*(23), 2229, doi:10.1029/2003GL018429.

La Hoz, C., and O. Havnes (2008), Artificial modification of polar mesospheric winter echoes with an RF heater: Do charged dust particles play an active role?, *J. Geophys. Res.*, *113*, D19205, doi:10.1029/2008JD010460.

Lehtinen, M. S., and I. Häggström (1987), A new modulation principle for incoherent scatter measurements, *Radio Sci.*, *22*, 625–634.

Li, Q., and M. Rapp (2013), PMSE observations with the EISCAT VHF- and UHF- radars: Ice particles and their effect on ambient electron densities, *J. Atmos. Sol. Terr. Phys.*, *104*, 270–276, doi:10.1016/j.jastp.2012.10.015.

Li, Q., M. Rapp, J. Röttger, R. Latteck, M. Zecha, I. Strelnikova, G. Baumgarten, M. Hervig, C. Hall, and M. Tsutsumi (2010), Microphysical parameters of mesospheric ice clouds derived from calibrated observations of polar mesosphere summer echoes at Bragg wavelengths of 2.8 m and 30 cm, *J. Geophys. Res.*, *115*, D00113, doi:10.1029/2009JD012271.

Mahmoudian, A., W. A. Scales, M. J. Kosch, A. Senior, and M. Rietveld (2011), Dusty space plasma diagnosis using temporal behavior of polar mesospheric summer echoes during active modification, *Ann. Geophys.*, *29*, 2169–2174, doi:10.5194/angeo-29-2169-2011.

Pinedo, H., C. La Hoz, O. Havnes, and M. Rietveld (2014), Electron-ion temperature ratio estimations in the summer polar mesosphere when subject to HF radio wave heating, *J. Atmos. Sol. Terr. Phys.*, *118*, 106–112, doi:10.1016/j.jastp.2013.12.016.

Rapp, M., and F.-J. Lübken (2000), Electron temperature control of PMSE, *Geophys. Res. Lett.*, *27*, 3285–3288.

Rapp, M., and F.-J. Lübken (2004), Polar mesosphere summer echoes (PMSE): Review of observations and current understanding, *Atmos. Chem. Phys.*, *4*, 2601–2633.

Rapp, M., et al. (2009), First in situ measurement of the vertical distribution of ice volume in a mesospheric ice cloud during the ECOMA/MASS rocket-campaign, *Ann. Geophys.*, *27*, 755–766.

Rietveld, M. T., H. Kohl, H. Kopka, and P. Stubbe (1993), Introduction to ionospheric heating experiments at Tromsø—I. Experimental overview, *J. Atmos. Terr. Phys.*, *55*, 577–599.

Rishbeth, H., and A. P. van Eyken (1993), EISCAT—Early history and the first ten years of operation, *J. Atmos. Terr. Phys.*, *55*(4–5), 525–542.

Robertson, S., et al. (2009), Mass analysis of charged aerosol particles in NLC and PMSE during the ECOMA/MASS campaign, *Ann. Geophys.*, *27*, 1213–1232.

Scales, W. (2004), Electron temperature effects on small-scale plasma irregularities associated with charged dust in the Earth's mesosphere, *IEEE Trans. Plasma Sci.*, *32*(2), 724–730, doi:10.1109/TPS.2004.826082.

Scales, W. A., and C. Chen (2008), On initial enhancement of mesospheric dust associated plasma irregularities subsequent to radiowave heating, *Ann. Geophys.*, *26*, 2265–2271.

Senior, A., M. T. Rietveld, M. J. Kosch, and W. Singer (2010), Diagnosing radio plasma heating in the polar summer mesosphere using cross-modulation: Theory and observations, *J. Geophys. Res.*, *115*, A09318, doi:10.1029/2010JA015379.

Turunen, E., P. N. Collis, and T. Turunen (1988), Incoherent scatter spectral measurements of the summertime high-latitude D-region with the EISCAT UHF radar, *J. Atmos. Terr. Phys.*, *50*, 289–299, doi:10.1016/0021-9169(88)90015-3.